AIAA 78-65R

Hypersonic Laminar Viscous Flow Past Spinning Cones at Angle of Attack

Ramesh Agarwal* and John V. Rakich†
NASA Ames Research Center, Moffett Field, Calif.

Computational results are presented for hypersonic viscous flow past spinning sharp and blunt cones at angle of attack, obtained with a parabolic Navier-Stokes marching code. The code takes into account the asymmetries in the flowfield resulting from spinning motion and computes the asymmetric shock shape, cross-flow and streamwise shear, heat transfer, cross-flow separation, and vortex structure. The Magnus force and moments are also computed. Comparisons are made with other theoretical analyses based on boundary-layer and boundary-region equations, and an anomaly is discovered in the displacement thickness contribution to the Magnus force when compared with boundary-layer results.

Nomenclature

c_p = specific heat at constant pressure divided by the freestream value
C_N = normal force coefficient
C_n = Magnus moment coefficient
C_{n_y}, C_{n_ϕ} = Magnus moment coefficient due to p_w and τ_ϕ, respectively
C_Y = Magnus force coefficient
$C_{Y_x}, C_{Y_y}, C_{Y_\phi}$ = Magnus force coefficient due to τ_x, p_w, and τ_ϕ, respectively

$$F_{\tau_x} = \sin^2\theta_c \int_0^x \int_0^{2\pi} x\sin\phi\,\tau_x(x,\phi)\,d\phi\,dx$$

$$F_{p_w} = \frac{\sin 2\theta_c}{2} \int_0^x \int_0^{2\pi} x\sin\phi\,p_w(x,\phi)\,d\phi\,dx$$

$$F_{\tau_\phi} = \sin\theta_c \int_0^x \int_0^{2\pi} x\cos\phi\,\tau_\phi(x,\phi)\,d\phi\,dx$$

h = static enthalpy divided by freestream value
L = reference length
M_∞ = freestream Mach number
p = pressure divided by twice the freestream dynamic pressure
p_w = wall pressure
Pr = freestream Prandtl number
r = metric for the ϕ coordinate; $x\sin\theta + y\cos\theta$
Re = freestream Reynolds number
S = Sutherland's constant
S_t = heat transfer coefficient
T_0 = freestream stagnation temperature, °R
T_w = wall temperature, °R
u, v, w = velocity in the x, y, and ϕ directions, respectively, divided by freestream velocity
V_∞ = freestream velocity
x = coordinate along the rays of the cone surface divided by L
y = coordinate normal to the surface divided by L
α = angle of attack
γ = ratio of specific heats
η = transformed normal coordinate
θ_c = cone half angle
μ = viscosity divided by freestream viscosity
ξ = bow-shock standoff distance divided by L
ρ = density divided by freestream density
τ_x = primary flow wall shear stress
τ_ϕ = cross-flow wall shear stress
ϕ = circumferential coordinate
Ω = angular velocity, rpm

Presented as Paper 78-65 at AIAA 16th Aerospace Sciences Meeting, Huntsville, Ala., Jan. 16-18, 1978; submitted Dec. 13, 1979; revision received Aug. 24, 1981. This paper is declared a work of the U. S. Government and therefore is in the public domain.

*NRC Research Associate. Presently Scientist at McDonnell Douglas Research Laboratories, St. Louis, Mo. Member AIAA.
†Research Scientist. Associate Fellow AIAA.

I. Introduction

HYPERSONIC viscous flow past a spinning projectile has been the subject of a number of theoretical as well as experimental investigations in the past because of its application in ballistics. Recently the problem, especially that of a blunt spinning body, acquired renewed interest because of its relevance in slow-spin planetary entry.

The very first analytical attempt to solve the boundary-layer equations for spinning bodies at an angle of attack was made by Sedney,[1] and most of the previous work on this problem has been summarized and discussed in recent papers by Dwyer and Sanders[2] and Lin and Rubin.[3] All the analytical and numerical work to date has been based on the boundary-layer equations; the exception is that of Lin and Rubin,[3] based on the boundary-region equations. In the boundary-layer analysis, the pressure gradient normal to the body surface is assumed negligible, making such an analysis valid only for very small angles of attack so that the normal component of velocity is small and there is no crossflow separation. In the boundary-region formulation, on the other hand, the pressure gradient in the body normal direction is balanced by the centrifugal forces. Both formulations require knowledge of the outer inviscid flowfield which is assumed to be conical and unaffected by rotation. The tabulated results of Jones[4] are used to obtain the outer inviscid flow.

In the present investigation, flowfields around sharp and blunt spinning cones at high angles of attack are computed by modifying the Lubard-Helliwell[5] parabolic Navier-Stokes marching code. In the parabolic approximation which has recently been employed by a number of investigators[6-9] for computing supersonic viscous flow, the viscous streamwise derivative terms are assumed small (therefore neglected) compared with the viscous normal and circumferential derivatives in the steady-state Navier-Stokes and energy equations. The resulting equations are of the parabolic type which permit a marching solution from an initial data surface. The code treats the flow between the body surface and the bow shock wave by these parabolized equations which are valid both in the viscous and inviscid flow regions. No assumption or knowledge about the outer inviscid flowfield is required. The code takes into account the asymmetries in the

flowfield resulting from spinning motion and computes the asymmetric shock shape, cross-flow and streamwise shear, heat transfer, cross-flow separation, and vortex structure. The Magnus force and moments are computed as well.

Employing the present parabolic Navier-Stokes approximation, new significant results about the nature of the Magnus force have been obtained which are at variance with the boundary-layer analyses even at small angles of attack. Sanders and Dwyer[10] as well as Lin and Rubin[3] have pointed out that four significant quantities contribute to the Magnus force: 1) pressure distribution due to asymmetric displacement thickness interactions; 2) centrifugal pressure gradient; 3) primary-flow wall shear; and 4) cross-flow wall shear.

In the boundary-layer and boundary-region approaches, calculation of the contribution to Magnus force due to displacement interaction effects is based on a two-step procedure. First, the computation of the asymmetric boundary-layer displacement thickness is performed. All the investigators have solved an approximate ordinary differential equation according to Moore[11] to obtain the three-dimensional displacement surface. This equation requires as input the displacement thickness quantities based on axial and circumferential velocity components whose calculation introduces further approximation. Second, the computation of pressure field on the new asymmetric body shape (composed of the original body plus the asymmetric displacement thickness) is done. Slender-body theory has been used for computing the pressure distribution by all the investigators except Sanders and Dwyer[10] who use a three-dimensional inviscid Eulerian code. This two-step procedure is avoided in the present approach. Furthermore, another important aspect is its applicability in computing cross-flow separation at high angles of attack.

II. Formulation of the Problem

A. Governing Equations

The governing equations are parabolized Navier-Stokes equations derived by Lubard and Helliwell[5] under the assumption that the gradients of the shear stress in the streamwise direction are negligibly small compared with the gradients in the normal and circumferential directions. In the development of these equations, a body-oriented coordinate system is used (Fig. 1), with x taken along a cone generator, y normal to the surface, and ϕ the circumferential coordinate where $\phi=0$ represents the windward ray. The coordinate system does not rotate with the body. The resulting nondimensional equations are given as follows.

Continuity

$$\frac{\partial(\rho ur)}{\partial x}+\frac{\partial(\rho vr)}{\partial y}+\frac{\partial(\rho w)}{\partial \phi}=0$$

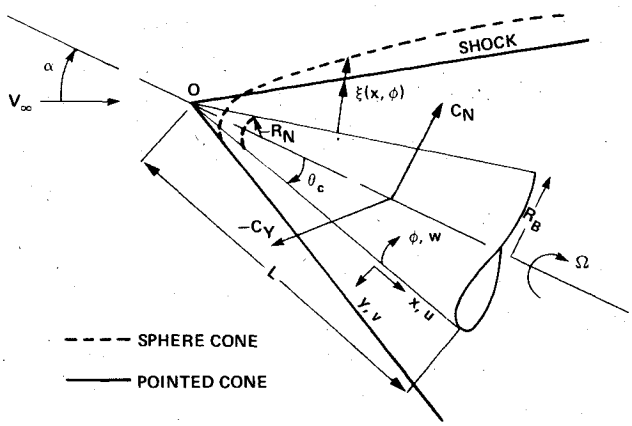

Fig. 1 Coordinate system.

x momentum

$$\frac{\partial(\rho u^2 r)}{\partial x}+\frac{\partial(\rho uvr)}{\partial y}+\frac{\partial(\rho wu)}{\partial \phi}-\rho w^2\sin\theta_c+r\frac{\partial p}{\partial x}$$
$$=\frac{r}{Re}\left[\frac{\partial}{\partial y}\left(\mu\frac{\partial u}{\partial y}\right)+\frac{1}{r^2}\frac{\partial}{\partial \phi}\left(\mu\frac{\partial u}{\partial \phi}\right)\right]$$

y momentum

$$\frac{\partial(\rho uvr)}{\partial x}+\frac{\partial(\rho v^2 r)}{\partial y}+\frac{\partial(\rho wv)}{\partial \phi}-\rho w^2\cos\theta_c+r\frac{\partial p}{\partial y}$$
$$=\frac{r}{Re}\left[\frac{4}{3}\frac{\partial}{\partial y}\left(\mu\frac{\partial v}{\partial y}\right)+\frac{1}{r^2}\frac{\partial}{\partial \phi}\left(\mu\frac{\partial v}{\partial \phi}\right)\right.$$
$$\left.-\frac{2}{3r}\frac{\partial}{\partial y}\left(\mu\frac{\partial w}{\partial \phi}\right)+\frac{1}{r}\frac{\partial}{\partial \phi}\left(\mu\frac{\partial w}{\partial y}\right)\right]$$

ϕ momentum

$$\frac{\partial(\rho uwr)}{\partial x}+\frac{\partial(\rho vwr)}{\partial y}+\frac{\partial(\rho w^2)}{\partial \phi}+\rho uw\sin\theta_c$$
$$+\rho vw\cos\theta_c+\frac{\partial p}{\partial \phi}=\frac{r}{Re}\left[\frac{\partial}{\partial y}\left(\mu\frac{\partial w}{\partial y}\right)+\frac{4}{3r^2}\frac{\partial}{\partial \phi}\right.$$
$$\left.\times\left(\mu\frac{\partial w}{\partial \phi}\right)+\frac{1}{r}\frac{\partial}{\partial y}\left(\mu\frac{\partial v}{\partial \phi}\right)-\frac{2}{3r}\frac{\partial}{\partial \phi}\left(\mu\frac{\partial v}{\partial y}\right)\right]$$

Energy

$$\frac{\partial(\rho uhr)}{\partial x}+\frac{\partial(\rho vhr)}{\partial y}+\frac{\partial(\rho wh)}{\partial \phi}-r(\gamma-1)M_\infty^2$$
$$\times\left(u\frac{\partial p}{\partial x}+v\frac{\partial p}{\partial y}+\frac{w}{r}\frac{\partial p}{\partial \phi}\right)=\frac{r}{RePr}\left[\frac{\partial}{\partial y}\left(\frac{k}{c_p}\frac{\partial h}{\partial y}\right)\right.$$
$$\left.+\frac{1}{r^2}\frac{\partial}{\partial \phi}\left(\frac{k}{c_p}\frac{\partial h}{\partial \phi}\right)\right]+\frac{(\gamma-1)M_\infty^2 r}{Re}\left[\mu\left(\frac{\partial u}{\partial y}\right)^2\right.$$
$$+\frac{\mu}{r^2}\left(\frac{\partial u}{\partial \phi}\right)^2+\frac{4}{3}\mu\left(\frac{\partial v}{\partial y}\right)^2+\frac{\mu}{r^2}\left(\frac{\partial v}{\partial \phi}\right)^2$$
$$+\mu\left(\frac{\partial w}{\partial y}\right)^2+\frac{4}{3}\frac{\mu}{r^2}\left(\frac{\partial w}{\partial \phi}\right)^2-\frac{4\mu}{3r}\frac{\partial v}{\partial y}\frac{\partial w}{\partial \phi}$$
$$\left.+\frac{2\mu}{r}\frac{\partial v}{\partial \phi}\frac{\partial w}{\partial y}\right]$$

Equation of state (perfect gas)

$$\rho=\gamma M_\infty^2(p/h)$$

Viscosity law (Sutherland's)

$$\mu=\frac{\sqrt{h}(1+S)}{1+S/h}$$

Prandtl number and specific heat are assumed constant.

B. Boundary Conditions

The following boundary conditions at the cone surface are used:

$$u=v=0;\quad w=w_B=\frac{2\pi}{60}\frac{\Omega L}{V_\infty}x\sin\theta_c$$

$$h_w = c_p T_w = \text{specified constant}$$

$$\left(\frac{\partial p}{\partial y}\right)_w = \frac{1}{Re}\left(\frac{4}{3}\mu\frac{\partial^2 v}{\partial y^2} + \frac{\mu}{3r}\frac{\partial^2 w}{\partial y \partial \phi}\right) + \frac{\rho w^2 \cos\theta_c}{r}$$

To obtain the outer boundary conditions, Rankine-Hugoniot conditions are utilized at the shock.

The components of freestream velocity in the body-oriented coordinate system are

$$u_\infty = \cos\theta_c\cos\alpha - \sin\theta_c\sin\alpha\cos\phi$$

$$v_\infty = -\sin\theta_c\cos\alpha - \cos\theta_c\sin\alpha\cos\phi$$

$$w_\infty = \sin\phi\sin\alpha$$

The Rankine-Hugoniot jump conditions then can be written as follows.

Conservation of mass

$$(u_\infty - \rho_k u_k)\frac{\partial \xi}{\partial x} - (v_\infty - \rho_k v_k) + (w_\infty - \rho_k w_k)\frac{1}{r}\frac{\partial \xi}{\partial \phi} = 0$$

Conservation of normal momentum

$$\frac{\left(u_\infty \frac{\partial \xi}{\partial x} - v_\infty + \frac{w_\infty}{r}\frac{\partial \xi}{\partial \phi}\right)^2}{\left(\frac{\partial \xi}{\partial x}\right)^2 + 1 + \left(\frac{1}{r}\frac{\partial \xi}{\partial \phi}\right)^2} + p_\infty$$

$$= \frac{\left(u_k \frac{\partial \xi}{\partial x} - v_k + \frac{w_k}{r}\frac{\partial \xi}{\partial \phi}\right)^2}{\left(\frac{\partial \xi}{\partial x}\right)^2 + 1 + \left(\frac{1}{r}\frac{\partial \xi}{\partial \phi}\right)^2} \rho_k + p_k$$

Conservation of tangential momentum

$$(u_\infty - u_k)\left[\frac{1}{r^2}\left(\frac{\partial \xi}{\partial \phi}\right)^2 + 1\right] + (v_\infty - v_k)\frac{\partial \xi}{\partial x}$$

$$-\frac{(w_\infty - w_k)}{r}\frac{\partial \xi}{\partial \phi}\frac{\partial \xi}{\partial x} = 0$$

$$(v_\infty - v_k)\frac{1}{r}\frac{\partial \xi}{\partial \phi} + (w_\infty - w_k) = 0$$

Conservation of energy

$$h_\infty + \frac{(\gamma-1)}{2}M_\infty^2 V_\infty^2 = h_k + \frac{(\gamma-1)}{2}M_\infty^2 (u_k^2 + v_k^2 + w_k^2)$$

The subscript k denotes the value of the variable just inside the shock. To uniquely determine the six unknowns ξ, u_k, v_k, w_k, p_k, h_k, the preceding five equations must be augmented with another equation which matches the shock to the state of the downstream flow. A one-sided differencing of the continuity equation provides the sixth equation.

Since the windward and leeward surfaces are not symmetry planes for the spinning cone, a periodicity condition for the flow profiles in the windward plane is specified.

In a rectangular y-ϕ grid the shock may not fall on a mesh point so that the mesh points would have to be moved or added to accommodate the shock. Thus, the transformation $\eta = y/\xi(x,\phi)$ is made. The resulting equations are then solved for $0 \le \eta \le 1$, $0 \le \phi \le 2\pi$, where $\eta = 0$ corresponds to the cone and $\eta = 1$ corresponds to the shock. The shock distance ξ appears in all the equations. To keep the matrix of coefficients obtained from the difference form of the equations in the block tridiagonal form, a sixth equation

$$\frac{\partial \xi}{\partial \eta} = 0$$

is differenced. Thus, the problem to be solved consists of six differential equations, six boundary conditions at each of the positions $\eta = 0$ and 1, and a periodicity condition for the flow profiles at $\phi = 0$ or 2π. With the specification of initial conditions, a marching scheme in x can be used to solve the equations.

III. Method of Solution

A. Numerical Scheme

Details of the numerical differencing scheme together with analysis of convergence and stability criteria are given in Helliwell and Lubard.[12] The differencing scheme used can be termed as implicit iterative. The normal derivatives are differenced completely implicitly at the new x station and new iterate. The circumferential derivatives are differenced at the new x station such that only the central and backward terms are taken at the new iterate. Newton's method of iteration is then used to solve the nonlinear algebraic equations which result from the differencing. It is known that this iteration procedure converges if the initial guess is close enough to the solution, and linearly extrapolating the solution at the previous two x stations seems to give a satisfactory initial guess. This numerical scheme of Helliwell and Lubard[12] imposes lower as well as upper bound restrictions on the step size Δx in the marching direction; there is an upper bound restriction on Δx for convergence and a lower bound restriction to avoid branching solutions. For a given Δx, it is usually not clear at the outset whether the solution is branching or is simply numerically unstable. According to Vigneron et al.[13] for certain values of Δx, numerical instability, as well as the branching of solution, can occur depending on whether the streamwise pressure gradient $\partial p/\partial x$ is backward differenced or evaluated implicitly. By a suitable choice of Δx, the present iterative method of solution seems effective in suppressing both the numerical instability and the branching of the solution. It is important to mention, however, that in some cases, completely neglecting the $\partial p/\partial x$ (which is justifiable in nearly conical flows) may be the only effective way of obtaining a solution. The selection of a proper large enough value of Δx for given Δy and $\Delta\phi$ can be considered basically a trial and error procedure. While running the code, if the stability problems arise, Δx is decreased; if the difficulties persist, $\partial p/\partial x$ should be neglected.

In all the computations presented in the paper, a nonuniform mesh of 81 grid points in the body normal direction η with clustering near both the body and the shock was used. In the circumferential direction ϕ, a uniform mesh with $\Delta\phi = 10$ deg was used. The influence of grid resolution on the accuracy of the solution was studied. Comparable accuracy was obtained for both 61 and 71 grid points in the η direction with $\Delta\phi = 10$ deg. In the η direction, grid clustering near both the body and the shock was achieved by using the analytical formula due to Roberts.[14]

B. Generation of Initial Conditions

The code requires as input the flow profiles and shock standoff distance at some initial station. For a sharp cone an approximate starting solution is obtained by constructing a suitable analytical shock shape from the shock angles due to

the flow past a locally tangent wedge. The inviscid flowfield between the cone and the bow shock is obtained by using Rankine-Hugoniot jump relations across the bow shock. Then an approximate Blasius type boundary-layer solution is constructed between the body and the bow shock, taking into account the spin on the body. Experience has shown that a fairly good starting solution is thus obtained even at very high angles of attack. For a sphere cone, the complete Navier-Stokes solution for a sphere due to Tannehill et al.,[15] is used at the sphere-cone junction. The Navier-Stokes solution for the sphere in the wind-oriented coordinate system is made suitable for the marching code (which employs a body-oriented coordinate system) by coordinate rotations.

IV. Results and Discussion

The results are presented in three parts for three sets of flow conditions. In part A, the flow conditions are those used by Sanders and Dwyer[10] in their boundary-layer analysis. Comparisons are made with their solution, and disagreement is found with their computation of the Magnus-force contribution due to displacement-thickness interactions. In part B, the flow conditions are those of Tracy's experiments.[16] Solutions for this case are obtained at very high angles of attack at which leeside vortices appear. In part C, the flow conditions are those of experiments by Cleary[17] for a sphere cone. Comparisons are made between blunt- and sharp-cone results for the same base Reynolds number. Because of lack of experimental data for the spinning cone for all three laminar flow conditions, the comparisons were made with the experimental data for zero spin rate. An excellent agreement was obtained with Tracy's sharp-cone experiment as well as Cleary's sphere-cone experiment.

A. Flow Conditions (Sharp Cone)

$$M_\infty = 4, \quad Pr = 1, \quad T_w/T_0 = 0.24, \quad \Omega = 30{,}000 \text{ rpm}$$

$$L = 30.48 \text{ cm (1 ft)}, \quad \theta_c = 10 \text{ deg}$$

$$Re = (2.81 \times 10^6 \text{ and } 2.81 \times 10^5), \quad \alpha = (2, 4, \text{ and } 6 \text{ deg})$$

Figures 2 and 3 show the variation of streamwise shear and cross-flow shear, respectively, around the circumference of the cone. The agreement between the present computations and that of Dwyer and Sanders'[2] boundary-layer results is fairly good.

Figure 4 shows the variation of streamwise shear force F_{τ_x}, cross-flow shear force F_{τ_ϕ}, and the net surface pressure force F_{p_w} contributions to the Magnus force with distance along the generator of the cone for various angles of attack. For a clockwise spin (looking from the base of the cone), a side-force moment is considered negative pointing toward the left side of the body as shown in Fig. 1. We notice that F_{τ_ϕ} (cross-flow shear contribution to Magnus force) varies monotonically with x. The net surface-pressure-force contribution to Magnus force F_{p_w}, on the other hand, changes sign at some distance x_s from the tip depending on the angle of attack. Thus F_{τ_ϕ} and F_{p_w}, which have opposite signs for $x<x_s$, become additive for $x>x_s$ when $\alpha = 2$ and 4 deg. This result contradicts the boundary-layer results which do not indicate any such change in the sign of F_{p_w} for $x>x_s$. Since F_{p_w} is the result of viscous-inviscid interactions due to spin, it appears that its sign reversal may be Reynolds number dependent.

In Fig. 5, the variation of F_{τ_x}, F_{τ_ϕ}, and F_{p_w} is shown with x for two Reynolds numbers for 4-deg angle of attack. At the lower Reynolds number there is no change in the sign of F_{p_w} with x and it is opposite to that of F_{τ_ϕ}. It appears that the change in the sign of F_{p_w} is a Reynolds number effect. F_{p_w} is the sum of contributions to the Magnus force due to displacement interaction effect and the centrifugal pressure gradient.

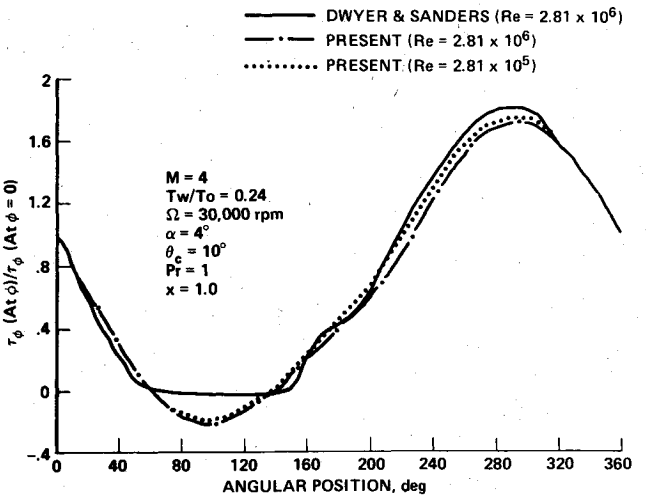

Fig. 2 Variation of primary flow wall shear relative to wind side.

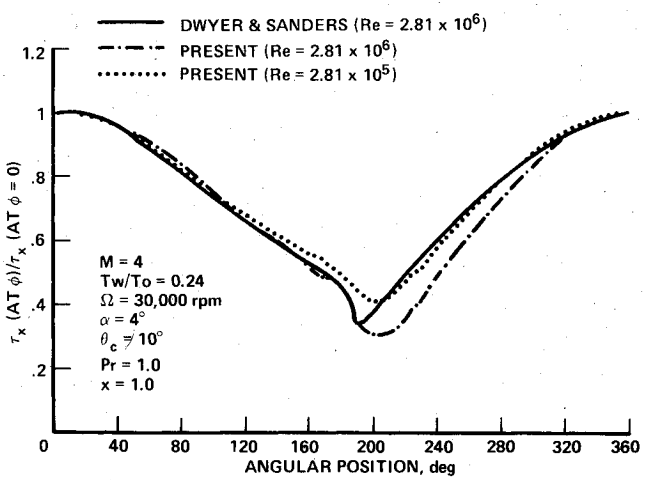

Fig. 3 Variation of cross-flow wall shear relative to wind side.

In Figs. 6 and 7, these two components of net surface pressure are plotted against the circumferential position at a typical streamwise location on the cone. Figure 6 shows that δp_c (centrifugal pressure difference $[p_c(\phi) - p_c(360 - \phi)]\cos\theta_c$) always has the same sign for all angles of attack so that its contribution to the Magnus force $\sim\int \delta p_c \sin\phi$ also has the same sign for all angles of attack. On the other hand δp_D (displacement pressure difference $[p_D(\phi) - p_D(360 - \phi)]\cos\theta_c$) changes sign along the circumference depending on the angle of attack so that its contribution to the Magnus force $\sim\int \delta p_D \sin\phi$ can be of the same sign or opposite to that due to δp_c, depending on the angle of attack. This point is more vividly illustrated by Fig. 7. For $\alpha = 4$ deg, δp_c has the same sign for both freestream Reynolds numbers, while δp_D changes sign. In Fig. 7, for the higher Reynolds number (2.81×10^6) case, δp_c and δp_D are also plotted near the tip at $x = 0.29$ where the local Reynolds number is less (8.15×10^5). δp_c and δp_D have the opposite sign just like the low Reynolds number (2.81×10^5) case at $x = 1$. From these results we conclude that it is the displacement-thickness interaction effect which is responsible for the sign of F_{p_w} and that the effect is dependent on the angle of attack and Reynolds number. The displacement-thickness effect contribution to the Magnus force is calculated very approximately in the usual boundary-layer analysis.

For this set of flow conditions, there are no experimental data available to verify these conclusions. Furthermore, in the experiments, it is not possible to isolate the contribution of various shear stresses and centrifugal and pressure forces to the Magnus force. Therefore, unless the net Magnus force on

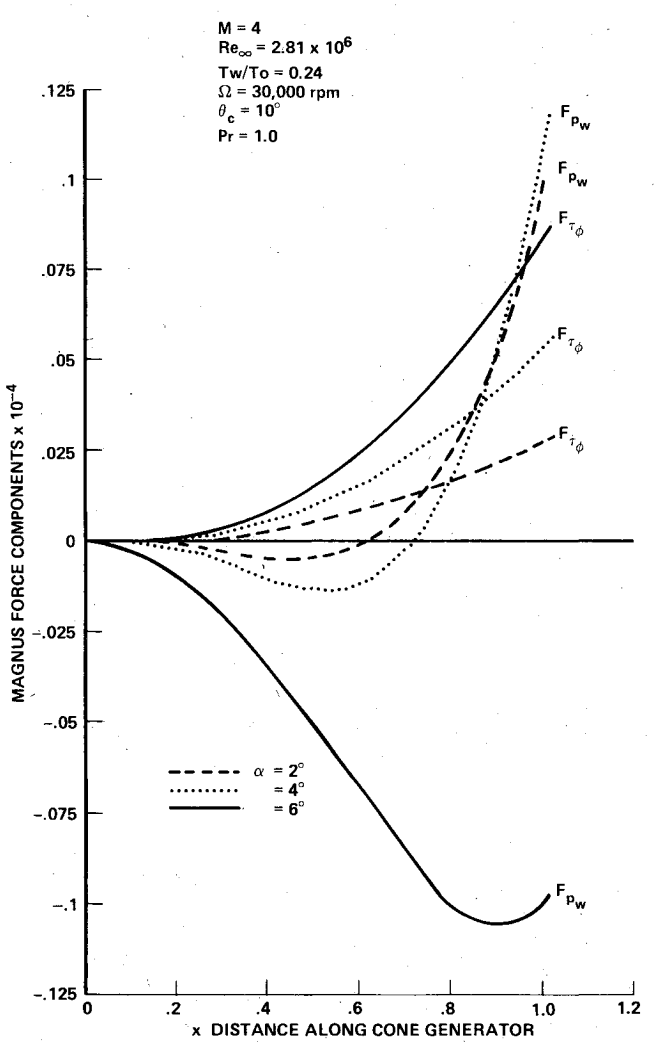

Fig. 4 Variation of Magnus force components with distance along the cone generator for various angles of attack.

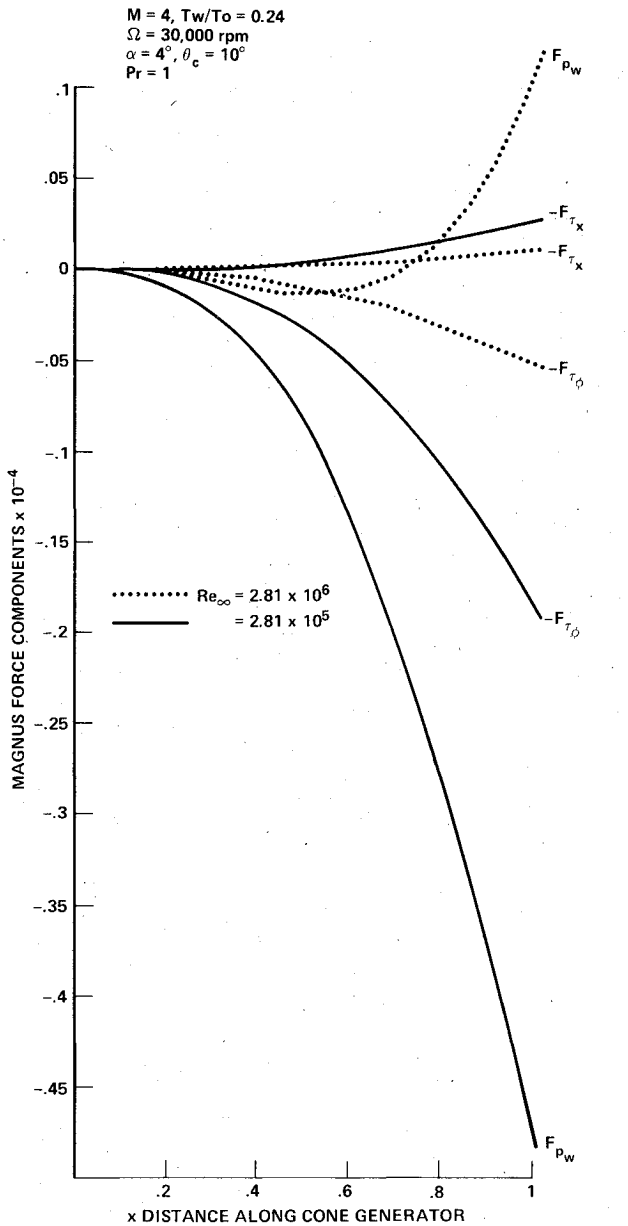

Fig. 5 Variation of Magnus force components with distance along the cone generator for various Reynolds numbers.

the body is of reverse sign (than conventionally expected), it is difficult to ascertain on the basis of experimental measurements of the Magnus force if the contribution of F_{p_w} has been of opposite sign than is conventionally expected. In the literature, reversed sign Magnus force has been reported by Dietrick[18] in low reduced-spin ($\Omega L/V_\infty$), and small angle-of-attack region from supersonic firing range data. Platou and Sternberg[19] also measured a reversed Magnus force at $M=2$ and $Re=0.65\times10^6$ for a body of noncircular cross section.

The whole viscous-inviscid interaction effect may be much more complicated and the sign of Magnus force may not simply depend on α/θ_c, Re, and $\Omega L/V_\infty$. In addition, it may be a function of other flow parameters; namely, M_∞ and T_w/T_0 as well. Of course, the transitional or turbulent flow, which is not the subject of the present paper, has large influence on the magnitude and direction of the Magnus force.[20,21]

In Fig. 8, the variation of Magnus force and moment coefficient with angle of attack is shown. A strong nonlinearity is obvious, a fact not brought out by the boundary-layer analysis of Sanders and Dwyer.[10] The result is explainable in light of the foregoing discussion. Furthermore, because of the small magnitude of the Magnus force in comparison to the normal force, it is also clear from our analysis that it is important to calculate accurately contributions due to all the boundary-layer forces. Figure 9 shows the change in the heat-transfer coefficient due to spin. Spin increases the heating in a small region on the leeside.

B. Flow Conditions (Sharp Cone)

$$M_\infty=7.95,\quad Pr=0.72,\quad T_w/T_0=0.4,\quad \Omega=10{,}000\text{ rpm}$$

$$L=10.16\text{ cm (4 in.)},\quad \theta_c=10\text{ deg},\quad Re=4\times10^5$$

$$\alpha=(4,8,12,\text{ and }16\text{ deg})$$

Figure 10 shows the variation of Magnus force and moment coefficient with angle of attack. Compare this figure with Fig. 8. The results for this case at small α are more like boundary-layer analysis results in contrast to case A where they are in contradiction with the boundary-layer theory. This is again explainable in terms of a Reynolds number effect. The Reynolds number for this case is an order of magnitude smaller than for case A.

At high angles of attack vortices appear on the leeside, a phenomenon dependent on the spin rate as well. Very high spin rates tend to suppress the vortex structure on the leeside. Figure 11 indicates the appearance of vortices at high angle of attack. The appearance of a vortex structure is indicative of flow separation; however, the cross-flow separation on a

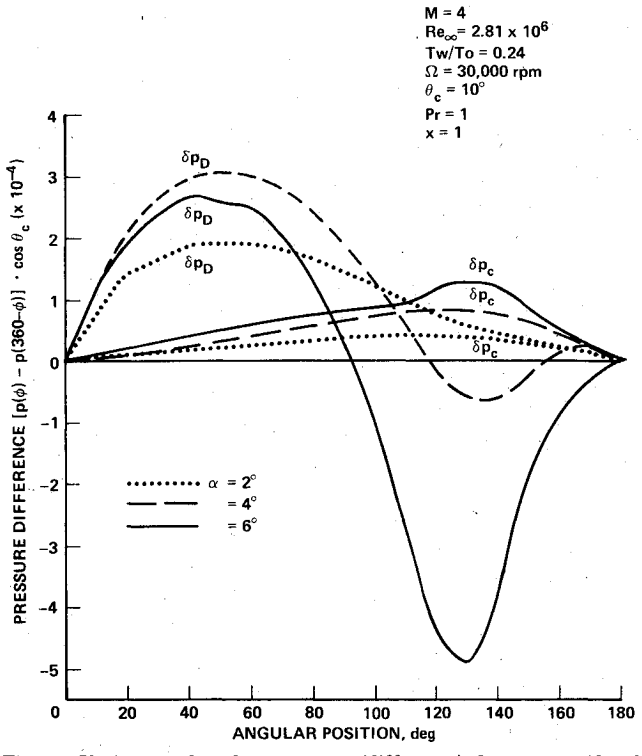

Fig. 6 Variation of surface pressure (difference) due to centrifugal effect (δp_c) and displacement effect (δp_D) around the circumference at $x=1$.

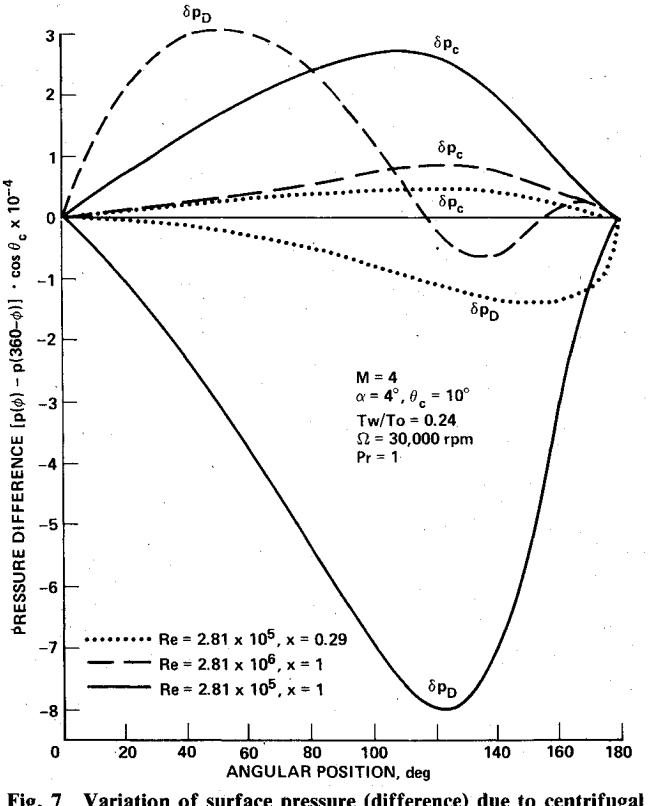

Fig. 7 Variation of surface pressure (difference) due to centrifugal effect (δp_c) and displacement effect (δp_D) around the circumference.

spinning cone is very different from that on a stationary one. In the cross plane, for spin in the clockwise direction, the external cross-flow is in the same direction as spin on the left side of the body, while on the right side of the body it is opposite to the direction of spin (Fig. 12). The onset of cross

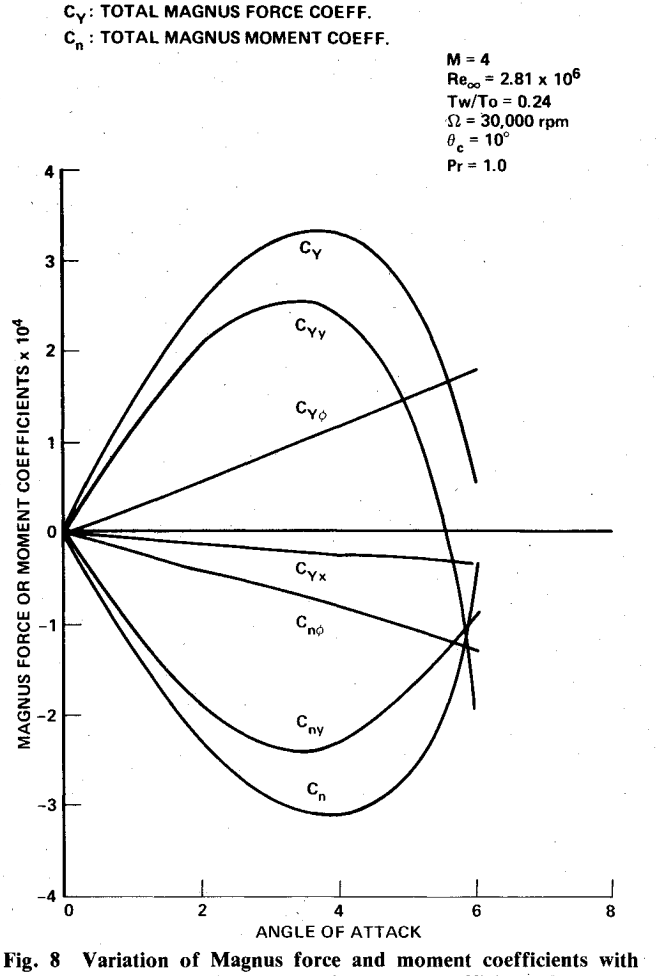

Fig. 8 Variation of Magnus force and moment coefficients with angle of attack (subscripts x, y, ϕ denote the coefficients due to τ_x, p_w, and τ_ϕ).

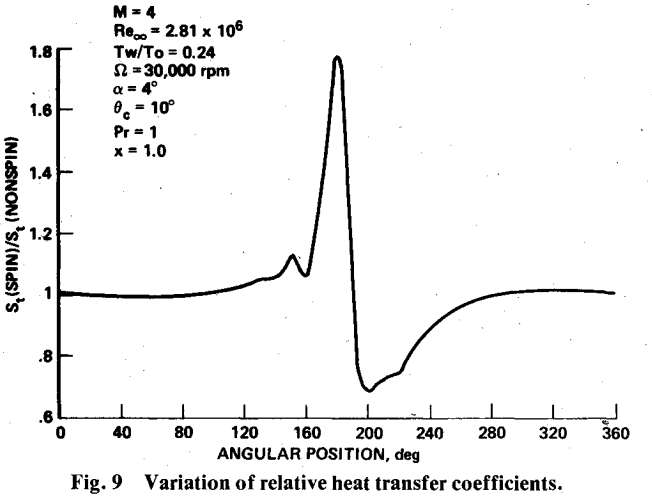

Fig. 9 Variation of relative heat transfer coefficients.

flow separation is defined by the condition $\partial w/\partial y = 0$ at $w = 0$ which occurs off the body surface. This condition encompasses the separation criterion for a nonspinning cone. In a generalized sense, separation means a reverse flow region, which for nonspinning bodies occurs next to the surface. In Fig. 13, the cross-flow velocity profiles in the separation zone on the leeside are shown for various values of α.

C. Flow Conditions (Sphere Cone)

$M_\infty = 10.6$, $Pr = 0.72$, $T_w/T_0 = 0.26$, $\Omega = 10{,}000$ rpm

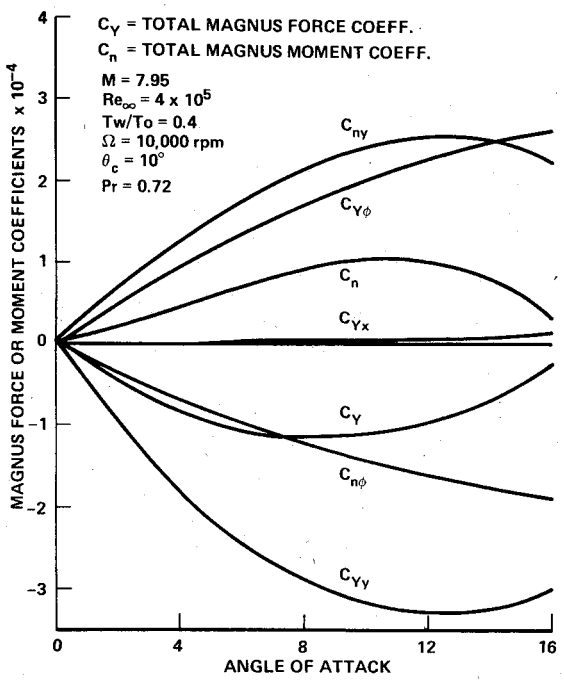

Fig. 10 Variation of Magnus force and moment coefficients with angle of attack (subscripts x, y, ϕ denote the coefficients due to τ_x, p_w, and τ_ϕ).

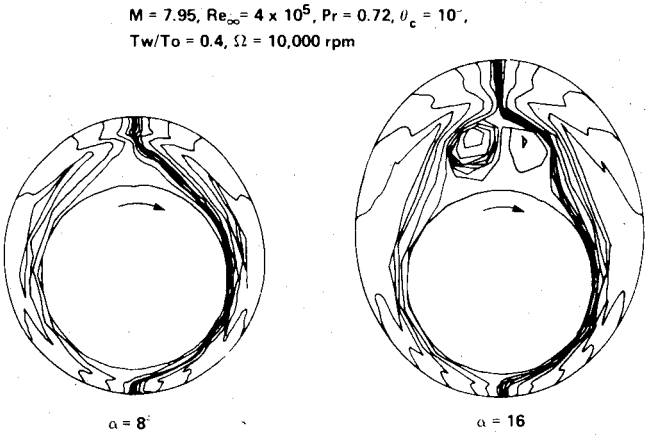

Fig. 11 Cross-flow velocity (w) contours in cross plane at $x = 1$ (normal coordinate has been artificially stretched to magnify the boundary-layer region).

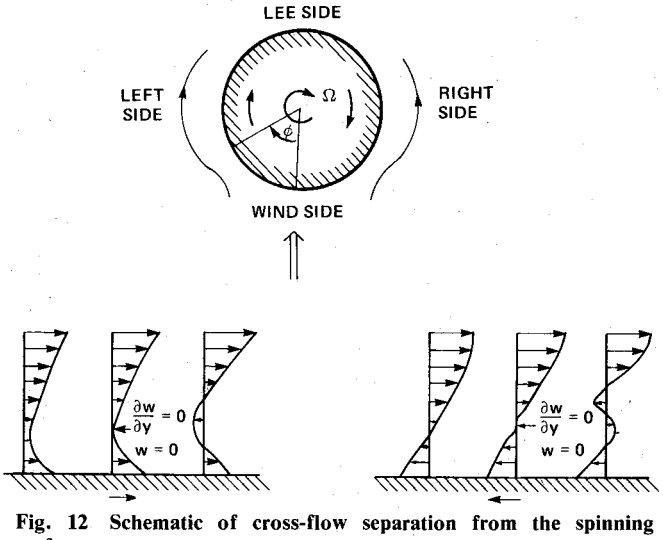

Fig. 12 Schematic of cross-flow separation from the spinning surface.

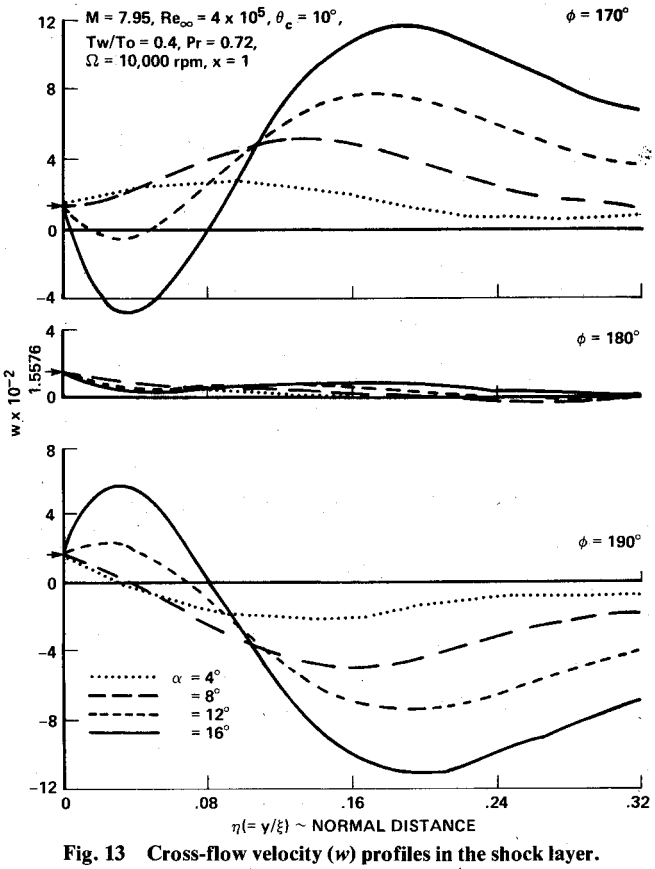

Fig. 13 Cross-flow velocity (w) profiles in the shock layer.

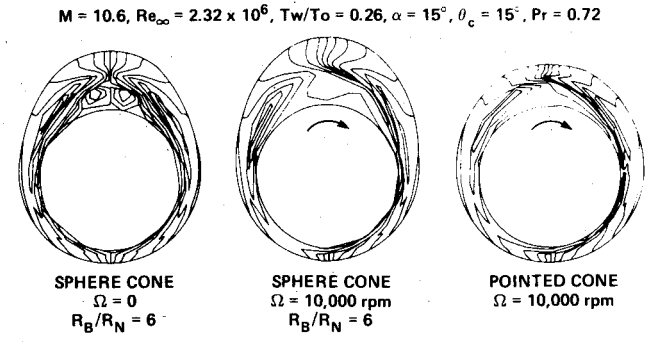

Fig. 14 Cross-flow velocity (w) contours in cross plane at $x = 1$ (normal coordinate has been artificially stretched to magnify the boundary-layer region).

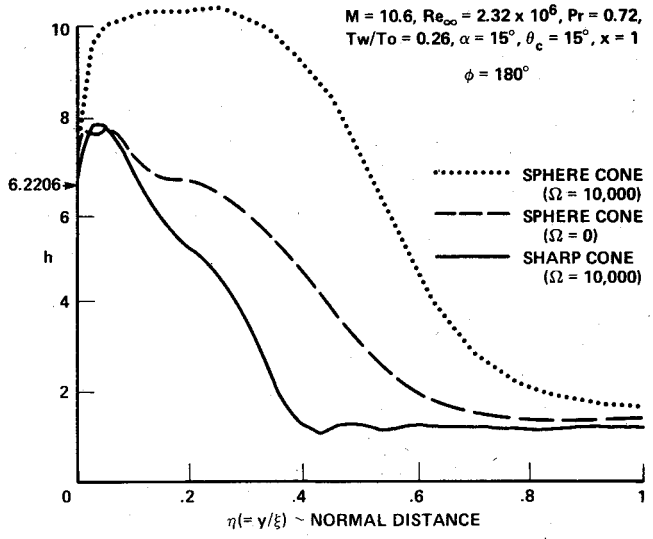

Fig. 15 Variation of static enthalpy in the shock layer.

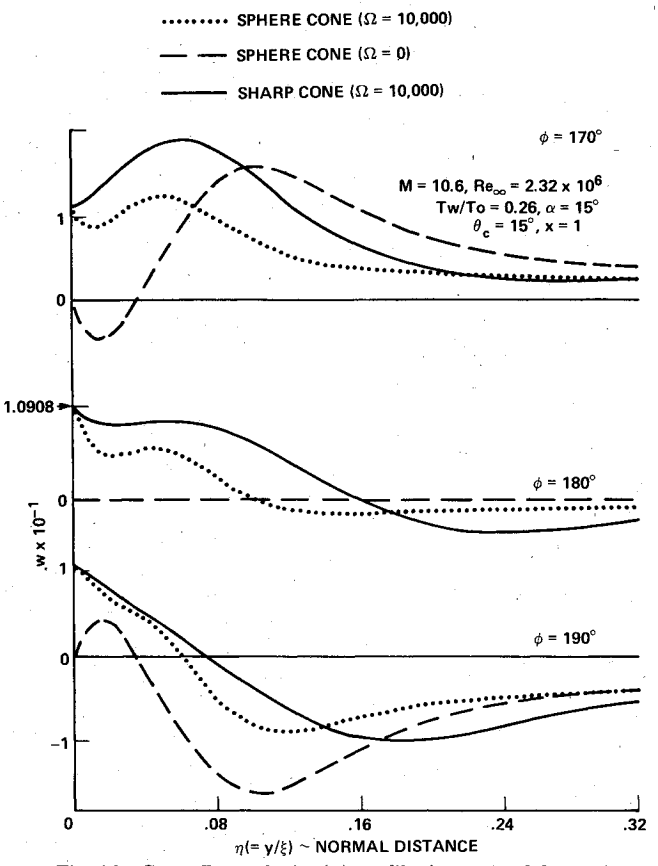

Fig. 16 Cross-flow velocity (w) profiles in the shock layer.

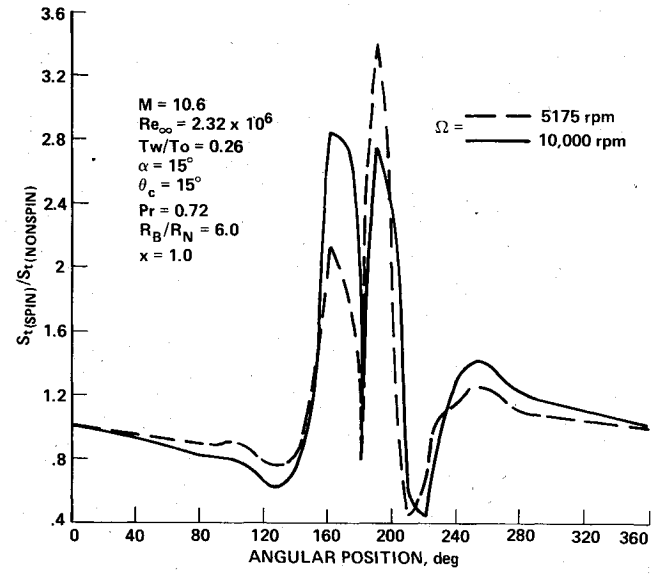

Fig. 17 Variation of relative heat transfer coefficients.

R_N (nose radius) = 2.54 cm (1 in.), R_B (base radius)/R_N = 6

$\theta_c = 15$ deg, $\alpha = 15$ deg

Re [(per meter) = 5.0×10^6] (per foot) = 1.2×10^6

Figure 14 shows the cross-flow velocity contours in a cross plane at $x = 1$ (base of the cone). When the spin rate is zero, there are two leeside vortices clearly exhibited. The high spin rate of 10,000 rpm prevents separation, a fact pointed out previously for the sharp cone. Also shown is the flow structure of a sharp cone of the same base diameter. The leeside structure of the shock layer is very different for a sphere cone and a sharp cone. As a result, the flowfield characteristics change dramatically in the leeside region due to slight bluntness, a point illustrated by showing the variation of static enthalpy on the leeside in the shock layer for a pointed as well as sphere cone (Fig. 15). In Fig. 16, the cross-flow velocity profiles in the cross plane in the leeside zone are presented to illustrate how the tendency toward separation is prevented by spinning the body. Figure 17 shows the change in heat-transfer coefficient around the circumference of the cone at $x = 1$ for two different spin rates. There is larger asymmetry in the profile for smaller spin rate because there is more tendency toward separation at smaller spinning velocities. These conclusions have important relevance for the slow-spin planetary entry problem.

V. Summary

In the present work, the flowfield of a spinning body at angle of attack has been calculated using the parabolized Navier-Stokes and energy equations approximation. The main results of this approach can be summarized as follows.

1) The contribution to Magnus force due to displacement interaction effects on the pressure field is at variance with that predicted by the boundary-layer theory both in magnitude and direction depending on the Reynolds number and spin rate even at small angles of attack. The correct calculation of the viscous-inviscid interaction effect is very important in order to have any meaningful results for the net Magnus force.

2) On the basis of results found in this study, the contribution due to cross-flow shear and centrifugal pressure gradient are of the same order of magnitude as that due to the displacement interaction effect, whereas the contribution due to primary flow wall shear is an order of magnitude smaller. This result is in agreement with the analyses of Sanders and Dwyer [10] as well as those of Lin and Rubin.[3]

3) At high angles of attack, leeside vortices which lift off the surface of a spinning body appear. The onset of cross-flow separation in the flowfield is characterized by $\partial w/\partial y = 0$ at $w = 0$.

4) Spin has a larger effect on the flowfield of a blunt body than on that of a pointed body, especially on the leeside.

5) Spin has a tendency to suppress the appearance of leeside vortices at high angle of attack.

References

[1] Sedney, R., "Laminar Boundary Layer on a Spinning Cone at Small Angles of Attack in a Supersonic Flow," *Journal of the Aerospace Sciences,* Vol. 24, June 1957, pp. 430-436.

[2] Dwyer, H. A. and Sanders, B. R., "Magnus Forces on Spinning Supersonic Cones—Part I: The Boundary Layer," *AIAA Journal,* Vol. 14, April 1976, pp. 498-504.

[3] Lin, T. C. and Rubin, S. G., "Viscous Flow Over Spinning Cones at Angle of Attack," *AIAA Journal,* Vol. 12, July 1974, pp. 975-985.

[4] Jones, D. L., "Tables of Inviscid Supersonic Flow About Circular Cones at Incidence $\gamma = 1.4$," AGARD 137, 1969.

[5] Lubard, S. C. and Helliwell, W. H., "Calculation of the Flow on a Cone at High Angle of Attack," R&D Associates, Santa Monica, Calif., RDA TR 150, Feb. 1973.

[6] Schiff, L. B. and Steger, J. L., "Numerical Simulation of Steady Supersonic Viscous Flow," AIAA Paper 79-0130, Jan. 1979.

[7] Rakich, J. V., Vigneron, Y. C., and Agarwal, R., "Computation of Supersonic Viscous Flows Over Ogive-Cylinders at Angle of Attack," AIAA Paper 79-0131, Jan. 1979.

[8] Helliwell, W. S., Dickinson, R. P., and Lubard, S. C., "Viscous Flows over Arbitrary Geometries at High Angle of Attack," AIAA Paper 80-0064, Jan. 1980.

[9] Bugglen, R. C., McDonald, H., and Kreskovsky, J. P., "Computation of Three-Dimensional Viscous Supersonic Flow in Inlets," AIAA Paper 80-0194, Jan. 1980.

[10] Sanders, B. R. and Dwyer, H. A., "Magnus Forces on Spinning Supersonic Cones—Part II: Inviscid Flow," *AIAA Journal,* Vol. 14, May 1976, pp. 576-582.

[11] Moore, F. K., "Displacement Effect on a Three-Dimensional Boundary Layer," NACA TN-2722, June 1952.

[12] Helliwell, W. S. and Lubard, S. C., "An Implicit Method for Three-Dimensional Viscous Flow with Application to Cones at Angle of Attack," *Computer and Fluids,* Vol. 3, March 1975, pp. 83-101.

[13] Vigneron, Y. C., Rakich, J. V., and Tannehill, J. C., "Calculation of Supersonic Viscous Flow over Delta Wings with Sharp Supersonic Leading Edges," NASA TM 78500, June 1978.

[14] Roberts, G. O., "Computational Meshes for Boundary Layer Problems," *Lecture Notes in Physics,* Springer-Verlag, New York, 1971, pp. 171-177.

[15] Tannehill, J. C., Holst, T. L., and Rakich, J. V., "Numerical Computation of Two-Dimensional Viscous Blunt Body Flows with an Impinging Shock," *AIAA Journal,* Vol. 14, Feb. 1976, pp. 204-211.

[16] Tracy, R. R., "Hypersonic Flow over a Yawed Circular Cone," Ph.D. Thesis, GALCIT Report, California Institute of Technology, Calif., Aug. 1963.

[17] Cleary, J. W., "Effects of Angle of Attack and Bluntness on Shock-Layer Properties of a 15° Cone at a Mach Number of 10.6," NASA TN D-4909, 1968.

[18] Deitrick, R. E., "Effect of a Hemispherical Base on the Aerodynamic Characteristics of Shells," Ballistic Research Laboratories (BRL) Rept. 947, Nov. 1955.

[19] Platou, A. S. and Sternberg, J., "The Magnus Characteristics of a 30 mm Aircraft Bullet," Ballistic Research Laboratories (BRL) Rept. 994, Sept. 1956.

[20] Fletcher, C. A. J., "Negative Magnus Forces in the Critical Reynolds Number Regime," *Journal of Aircraft,* Vol. 9, Dec. 1972, pp. 826-833.

[21] Sturek, W. B., Dwyer, H. A., Kayser, L. D., Nietubicz, D. J., Reklis, R. P., and Opalka, K. O., "Computations of Magnus Effects for a Yawed, Spinning Body of Revolution," *AIAA Journal,* Vol. 16, July 1978, pp. 687-692.